(2):715～724.

7 Boustie M, Cottet F. Experimental and numerical study of laser induced spallation into aluminum and copper targets. J Appl Phys,1991,69(11):7533～7538.

8 Larson A R. Calculation of laser induced spall in aluminum targets,LA 6189M,1975.

9 Fox J A, Barr D N. Laser－induced shock effects in plexiglass and 6061－T6 aluminum. Appl Phys Lett, 1973,22(11):594～596.

10 Shoukry M, Nair S, Kalpakjian S. Effect of shear deformation on the dynamic plastic bending of metallic plates during normal penetration. Int J Engng Sci, 1991,29(9):1035～1052.

11 Anderson C E, Bodner S R. Ballistic impact:the status of analytical and numerical modeling. Int J Impact Engng, 1988,7(1):9～35.

12 Liss J, Goldsmith W, Kell J M. A phenomenological penetration model of plates. Int J Solids Struct, 1983,1(2):321～341.

13 Jenq S T, Goldsmith W, Kell J M. Effect of target bending in normal impact of a flat－ended cylindrical projectile near the ballistic limit. Int J Solids Struct. 1988,24(2):1243～1266.

14 Duan Z P, Zhou Y C, Xie B M. On laser－induced reverse plugging effect, In: Zheng,Z M. In Proceedings of IUTAM Symp on Impact Dyn. peking:Peking University Press,1994,176～186.

15 Zhou Y C, Duan Z P. Shear deformation analysis of laser－induced reverse plugging effect, Submitted to Int J Non－Linear Mechanics,1996.

16 Berger H M. A new approach to the analysis of large deflections of plates. J Appl Mech, 1965,22:465～742.

17 Ohnable H, Mizuguchi F. Larger deflections of heated nonhomogeneous circular plates with radial varying rigidity. J Non－Linear Mech, 1993,28:365～372.

18 Bhimaraddi A, Chandrashekhara K. Nonlinear vibrations of heated antisymmetric angle－ply laminated plates. Int J Solids Structures, 1993,30:1255～1268.

博士论坛

一种新的破坏模式:反冲塞*

周益春[1,2) 段祝平[2) 杨奇斌[1)

【摘要】 观察到了长脉冲激光束辐照到铜薄片上产生的新的破坏模式.这种破坏可以分为三个阶段:鼓包,剪垣变形局部化及由冲塞所引起的贯穿,这种破坏模式的典型特征是鼓包和冲塞都是沿着入射激光相反的方向进行的,它同人们所塾知的激光引起材料破坏的分裂、烤化和汽化等不同,激发束的特殊的空间分布造成了这种新的破坏模式.

主题词:激光;破坏;反冲塞

分类号:TN249

* 国家 863 计划资助项目

作者单位:1)湘潭大学物理系,湘潭,411105;2)中国科学院力学研究所,材料动力学及激光与物质相互作用实验室

收稿日期:1996－05－06

(第 18 卷完)

DOCTOR'S FORUM

A NEW KIND OF DAMAGE: REVERSE PLUGGING*

Zhou Yichun[1),2)] *Duan Zhuping*[2)] *Yang Qibing*[1)]
([1)]Department of Physics, Xiangtan University, Xiangtan Hunan. 411105 China)
([2)]Laboratory for Laser and Dynamic Behaviors of Materials Institute of Mechanics, CAS, Beijing, 100080, China)

【Abstract】 A new kind of failure mode is observed in circular brass foils which their peripheries are fixed and their surfaces are subjected to a long pulsed laser over a central region. The failure is classified into three stages; they are referred to as thermal bulging, localized shear deformation and performation by plugging. A distinct feature of the failure mode is that bulging and plugging occurred in the direction opposite to the incident laser beam. The failure mode is different from the well—known types of laser induced material damage, such as spallation, melting and/or vaporization. The distinct feature of the spatial distribution of the laser intensity induces the nwe kind of failure mode.

Subject words: Laser, reverse plugging, damage

0 Introduction

High power laser has attracted a great deal of attention over the last few years, for those working in the fields of materials and/or structure damage and laser processing. Depending on the intensity and concentration of a laser beam over a solid, material damage could occur by spallation, melting and/or vaporization[1]. When the intensity of the continuous wave laser is about $10^3 W/cm^2$, there is the potential of failure by themal stress[2]. The damage may occur by melting and/or vaporization for the intensity of the order of $10^5 \sim 10^8 W/cm^2$ and the pulse duration of the order lof milliseconds[3-5]. In this case, the thermal stress concentrated around the crater plays an important role in material and/or structure damage. The formation of plasma may generate shock waves propagating into the materials for the intensity of the order of $10^8 \sim 10^{10} W/cm^2$ and the pulseduration of the order of nanoseconds. When wave reflection takes place between two surfaces, there is the potential of failure by spallation[6-9].

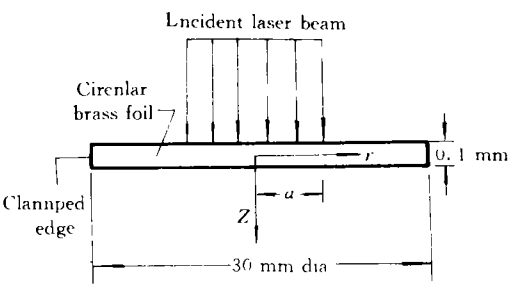

Fig. 1 Schematic of a normal incident laser beam impinging on a circular brass foil specimen

Besides the above mentioned types of damage, there is a new failure mode for non—

Gaussian laser beam in spatial feature. Those situations prevail where the size and inteneity of the laser beam are such that the spatial structure effect will contribute to the mode of failure such as bulging followed by plugging. Such are the cases considered in this investigation.

1 Experimental Procedure

Consider an incident laser beam that impinges normally on a circular brass foil as shown in Fig. 1. The $z-$and $r-$direction are aligned normal and parallel to the specimen whose edge is clamped. Let $2a$ denote the diameter of the laser spot that can vary from 2mm to 6mm . The foil has a diameter of 30mm and thickness of 0. 1mm . The brass material contains 65% copper, 33. 6% zinc, 0. 03% iron, 0. 06% antimony and other microelements that are negligibly small in percentage by weight.

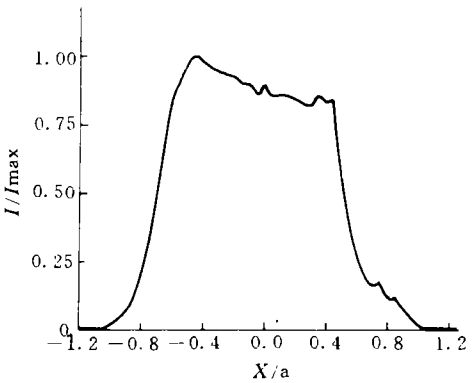

Fig. 2 Temporal shape of Nd:grass pulsed laser intensity

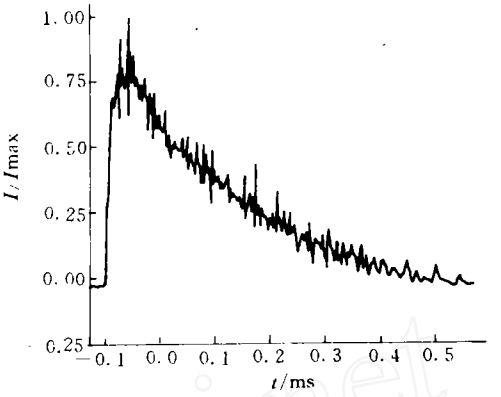

Fig. 3 Spatial shape of Nd:grass pulsed laser intensity

The energy of the laser beam ranges from 25J to 40J with an intensity of the order of 10^5 to $10^6 W/cm^2$. It is a single pulse Nd:grass laser with a wavelength of 1. 06μm. The diagnostics of the laser parameters provide a traditional monitoring of the laser beam characteristics, such as energy, temporal and spatial shapes. Displayed in Fig. 2 is the normalized intensity I/I_{max} with time. The normalized intensity I/I_{max} with space coordinates r/a is shown in Fig. 3, where r and a are, respectively, the radial distance and the radius of the laser spot. The full width at half maximum of the laser is approximately 250μs. The laser intensity rises rapidly within 50μs and then decays exponentially with a sawtooth oscillation. The spatial distribution of the laser intensity is non−Gaussian but roughly uniform within the laser irradiated region and declines very sharply towards the edge where the laser spot terminates. For the convenience of numerical analysis, the laser intensity I is approximated by

$$I=I_{max}e^{-\alpha t}(1-e^{-\beta t})f(r)=I_{max}g(t)f(r) \tag{1}$$

where α and β are determined experimentally test, and equal to 1.5×10^4/s and 8.0×10^4/s, respectively. Therefore, laser energy $E_J=\beta\pi a^2 I_{max}/\alpha(\alpha+\beta)$ and we have

$$f(r)=\begin{cases}1, & \text{if } 0\leqslant r\leqslant a\\ 0, & \text{if } a<r<\infty\end{cases} \tag{2}$$

and $f(r)=e^{-(r/a)^2}$ to account for the non−Gaussian and Gaussian nature of the laser beam,

respectively.

2 Experimental Results

2.1 Macro—phenomena

2.1.1 **Description of failure mode** Illustratedustrated schematically in Fig. 4 is the

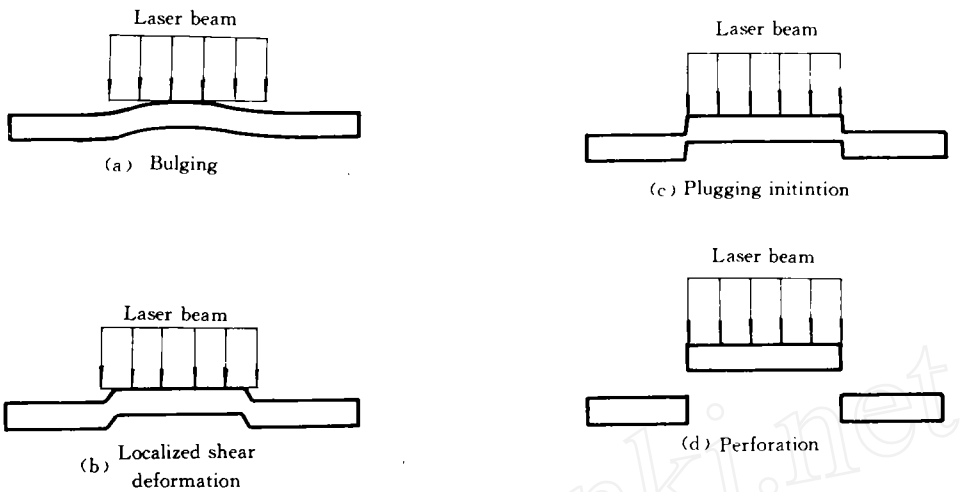

Fig. 4 Schematic of damage evolution:

evolution of specimen failure. Fig. 4(a) shows bulging of the brass foil at the earlier stage of laser irradiation. Note that this occurs towards the side of the incident laser beam where the temperature would be higher. Considerable shear deformation occurs around a rim near the outer edge of the laser beam which is shown in Fig. 4(b). This leads to the softening of the material due to intense heating.

Further intensification of the energy around the periphery of the laser beam leads to the initiation of plugging and final perforation which are shown in Fig. 4(c)—(d), respectively. The plugging mode of failure is customarily known to be associated with metal projectiles penetrating through metal targets in plate form[10—13]. A plug of the target material is ejected in the direction of the energy source that is the moving projectile. In the case of an incident laser beam, plugging occurred opposite to the incoming direction of the energy source. The initial bulge occurs on the side with higher temperature that determines the direction of plugging

2.1.2 Threshold intensity According to the test date in this study, when the laser energy density is lower than 151J/cm^2, or equivalently, the laser intensity is less than 0.51×10^6W/cm^2, no visible macroscopic damage was observed on the front or rear surface of the brass specimen. When the laser intensity is increased to 0.56×10^6W/cm^2, the bulging of brass specimen is observed. A slight melting is observed on the front surface at the periphery of the laser spot. The laser intensity threshold value I_{cr} for plugging to occur is about 0.61×10^6W/cm^2. As I exceeds I_{cr}, local melting of the material begins to take place. When the

laser intensity is increased to $0.75\times10^6W/cm^2$, the brass foil is totally fractured and fragmented. A study on laser－induced spallation in 0.1mm thick copper foil has been made in [6]. The intensity was of the order of $5.3\times10^{10}W/cm^2$; it is different five orders of magnitude to failure by plugging which is about $0.71\times10^6W/cm^2$. The thresholds for the laser en

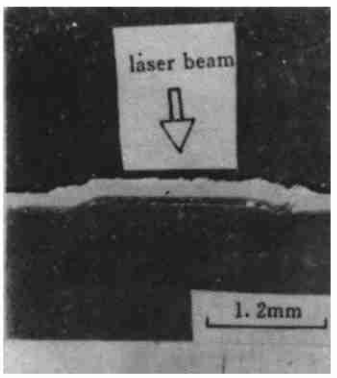

Fig. 5 Photo of sectioned brass foil at the bulge state with a laser energy of 8.2J over an area of 2.3mm in diameter

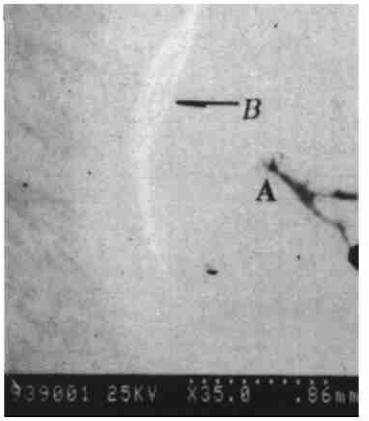

Fig. 6 Photo of brass foil failure by plugging viewed from the rear surface with a laser energy of 29J over region 4.5mm in diameter

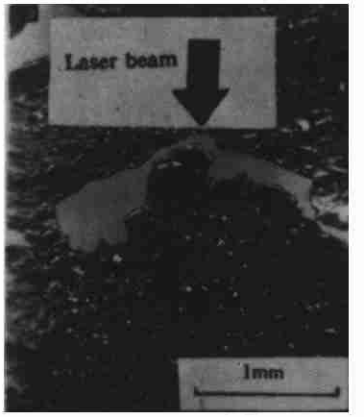

Fig. 7 Photo of fractured and fragmented brass foil subjected to a laser energy of 2.9J over region 2.3mm in diameter

ergy do not distinguish the two different faiure modes as they are both approximately equal to $210J/cm^2$.

2.1.3 Damage evolution The photo of a polished section of brass speciment is shown in Fig. 5 bulging in the direction opposite to the laser beam is observed with a maximum center deflection of 0.03mm. This corresponded to a laser energy of 8.2J; an intensity greater than $0.61\times10^6W/cm^2$; and a spot dimeter of 2.3mm. Softening of the material prevailed around the outer edge of the laser spot.

When the lser intensity is increased to $0.61\times10^6W/cm^2$, the plugging begins to take place in brass foil. Fig. 6 shows the circular brass foil failed by plugging opposite to direction of incident laser beam.

When the intensity is increased to $0.75\times10^6/cm^2$ the brass foil is totally fratured and fragmented. Fig. 7 shows a sectioned of fractured and fragmented brass foil subjected to a laser energy 9.2J over region 2.3mm in diameter.

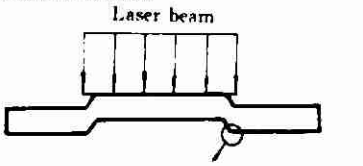

Fig. 8 Photo of cracks viewed from the rear surface, microcracks marked with arrow *B* and macrocracks marked with arrow *C* appeared on the surface and then growing in the circumferential direction.

2.2 Micro—phenomena

2.2.1 Cracks The micro - and macro - cracks by plugging are shown in Fig. 8. This corresponded to a laser energy of 29J;and a spot diameter of 4.5mm. The microcracks and macrocrack in the peripheral region are,respectively, marked with arrow *B* and *C* in Fig. 8.

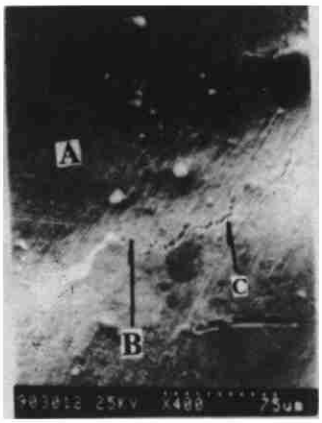

Fig. 9 Photo of sectioned brass foil for the initiation of microcrack, as marked with arrow *A*, on the rear surface and then growing in the thickness direction.

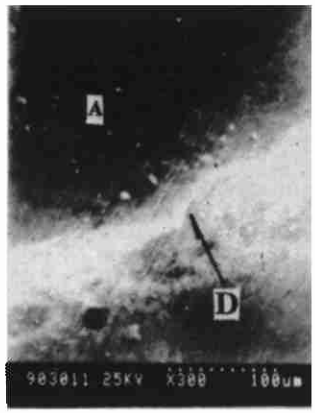

(a) fractographs caused by plugging;

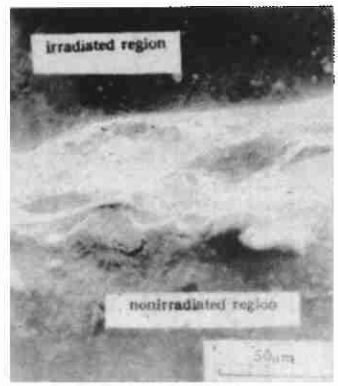

(b) enlargement of area *D* in photo of Fig. 10(a); The region marked by A in Fig. 10(a) denotes the rear surface of brass foil and its front surface is subjected to a laser energy of 31J over region 4.5mm in diameter.

Fig. 10 Photos of fractographs viewed from the rear surfaces

(a) fractograph in brass foil subjected to a laser energy of 29J over region 4.5mm in diameter;

(b) fractograph in 1.0mm thick brass plate perfected by 10cm length metal projectile which moved with velocity of 4.79m/s.

Fig. 11 Photos of fractographs induced by plugging;

Fig. 9 shows the microcrack on the rear surface at the periphery of the laser spot. Photos shown in Figs. 8 and 9 show that increased laser intensity lead to the initiation of microcracks in the peripheral region with radius $r \sim a$. The macrocracks appeared on the rear surface and then spread into the material. They would grow and coalesce into macrocracks that grow rapidly in the circumferential direction as well as in the thickness direction.

2. 2. 2 Fractographs The fractographs by plugging are shown in Fig. 10. This correspond to a laser energy of 29J; and a spot diameter of 4. 5mm . Fig. 10(a) shows the fractograph in circular brass foil failed by blugging opposite to direction of incident laser beam. Also the photo of the enlargement of aera *D* in the photo of Fig. 10(a) is shown in Fig. 10(b). One can see from the photos that the fractographs look like landslide, i. e, the profile of the snake—like pattern. They are typical plugging—type fractographs.

In addition, the fractographs induced by laser beam plugging and by metal projectile penetrating are shown in Fig. 11(a) and 11(b),respectively. Photo shown in Fig. 11(a) corresponded to a laser energy of 29J;and a spot diameter of 4. 5mm. Photo shown in Fig. 11 (b) corresponded to 1. 0mm thick brass plate perfected by 10cm length metal projectile which moved with velocity of 4. 79m/s. The experiment was carried using a split Hopkinson pressure bar . The characteristics for the fractographs do not distinguish the two different failure modes.

2. 3. 3 Plastic deformation At the periphery of the laser beam, the photos for the grain fining on the front and rear surfaces are shown in Figs. 12 (a) and 12(b),respectively.

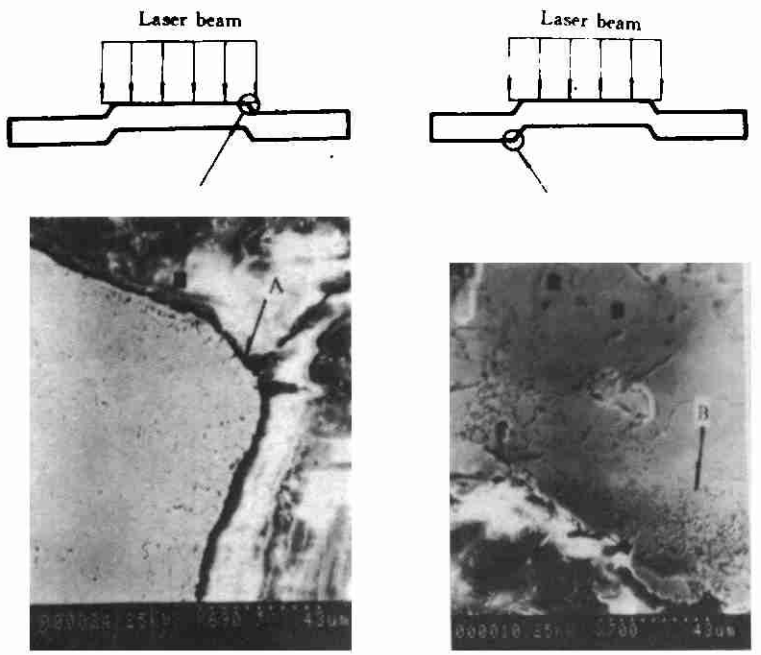

(a) grain fining on the front surface at the periphery of the laser spot (b) grain fining on the rear surface at the periphery of the laser spot.

Fig. 12 Photos of sectioned brass foil for grain fining

However, the grain fining does not take place within the irradiated region and in the mediate region at the periphery of the laser spot. The grain fining means that the finite plastic deformation occurs on the rear surface at the periphery of the laser spot. The fact that the finite

plastic deformation and the microcracks occur in the same region implies that the finite plastic deformation leads to the initiation of microcracks.

3 Discussions

The observed plugging failure of the brass foil specimen subjected to the Nd:grass long pulsed laser can be summarized in three stages.

Stage 1—The brass foil bulges towards the laser beam. At the earlier stage of laser irradiation, the deformation of the brass foil is infinitesimal and the classical Kirchhoff plate theory can be used to determine the defflection $w(r,t)$, then we have the equivalent transverse loading q_θ as[14]:

$$q_\theta = -\frac{1}{1-\upsilon}\nabla^2 M_T \tag{3}$$

where M_T is the thermal moment

$$M_T = \alpha_0 E\int_{-h/2}^{h/2}\theta(r,z,t)z\mathrm{d}z \tag{4}$$

and υ, E, α_0 and hare ,respectively, Poisson ratio, Young's modulus, the thermal expansion

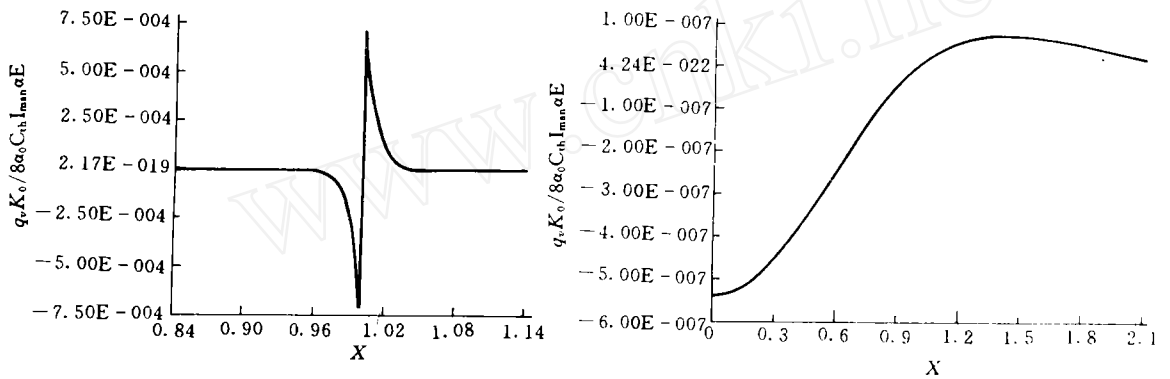

(a) or Gaussian (b) laser beam.

Fig. 13 Spatial distribution of equivalent transverse loading induced by either non—Gaussian

coefficient and the brass foil thickness. In the above expressions, $\nabla^2 = \frac{\mathrm{d}^2}{\mathrm{d}r^2} + \frac{1}{r}\frac{\mathrm{d}}{\mathrm{d}r}$ is the Laplace operator and $\theta(r,z,t)$ is the temperature rise.

A high temperature state is bult up on the specimen front surface impinged by a normal incident laser beam. This means that the temperature gradient in z—direction, i. e, $\frac{\partial\theta}{\partial z}$ or M_T is high at the earlier stage of laser irradiation and that tends to zero at the late stage of laser irradiation. The spatial profile of M_T is almost as same as that of laser beam. The numerical computations for the equivalent transverse loading q_θ are, respectively, shown in Figs. 13(a) and 13(b)in the cases of non—Gaussian and Gaussian laser beam. The spatial profile of M_T causes that q_θ is constantly negative in the irradiated region and q_θ is constantly positive near the outer edge of the laser beam. However, in the case of metal projectiles penetrating through metal targets in plate form, the transverse loading is constantly positive and zero

within and around the projectiles penetrating region, respectively. The negative value of q_θ within the irradiated region causes the foil to bulge towards the direction opposite to laser irradiation.

Stage2—High shear deformation occurs around a rim near the outer edge of the laser beam. A steep temperature gradient prevails across the periphery of the laser beam where the spot terminates. The distinct feature of the spatial distribution of the laser intensity causes the distinct feature of the spatial distribution of the equivalent transverse loading as shown in Fig. 13(a). The variation of q_θ with r/a in both cases is evidently different. The equivalent transverse loading q_θ varies with r/a in the peripheral region much more sharply in the non—Gaussian case than in the case of Gaussian type of laser.

To analyse the shear deformation in this study, we investigate the nonlinear response of heated, non—homogeneous circular plates[15]. Based on the large deflection equations of Berger[16], Ohnable and Mizuguhi[17] and the parabolic shear deformation theory of Bhimaraddi and Stevens[18], we have derived new coupled governing equations of shear deformation and deflection. The new equations are solved with the boundary condition of the edge clamped by the Galerkin method and the iterative method. Fig. 14 shows the transient average shear strain γ distributions with $E_J = 10$J at different time in the case of $D=D_0=D_0$ for the non—Gaussian and Gaussian types laser beam, where $D=\frac{Eh^3}{12(1-\upsilon^2)}$ is the bending rigidity and D_0 is the corresponding material parameters at room temperature. It is seen that only the shear strain γ is not zero in the peripheral region for the non—Gaussian laser beam. Comparing the shear strain distribution in brass foils induced by non—Gaussian type laser beam with that induced by Gaussian type laser beam, the former offers a formidable potential for the new type of faiure by plugging, however, the latter has a litter potential for the new type of failure by plugging. The transient average shear strain distributions are shown in Fig. 15 for the non—Gaussian type laser beam with $E_J=10$J at different time in the case of $D\neq D_0$. The average shear strain in the case of $D\neq D_0$ is much larger than that in the case of $D=D_0$. This means that the shear

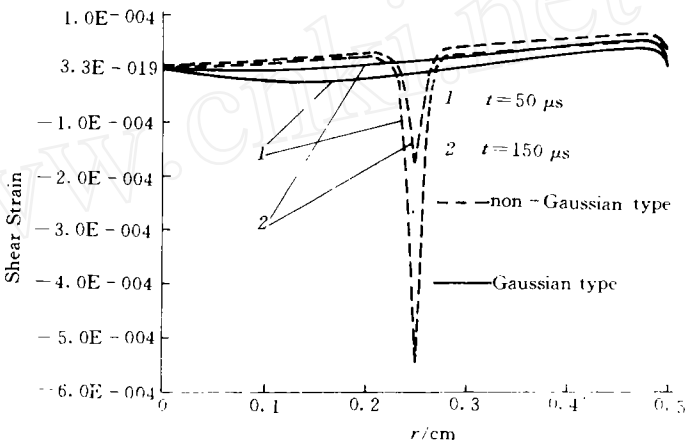

Fig. 14 Transient average shear strain γ vs the radial coordinate for the non—Gaussian and Gaussian types of laser beam with $E_J=10$J at different time in the case of $D=D_0$.

deformation comes under the strong influence of the dependence of the Young's modulus E (T) on temperature T.

As a whole the distinct feature of the spatial distribution of the laser intensity causes the shear strain at the periphery of the laser spot is much larger than that in other region . High shear deformation concentrated in a rim is developed and causes a circular region impinged upon by the laser to move further in the bulged direction.

Stage 3—When the laser intensity reaches a critical value, failure by plugging takes place opposite to the direction of the incident laser beam.

On a microscopic scale, the plugging failure characteristics induced by a laser are similar to those found in brass plates perfected by metal projectiles. Such experiments are well known and have been carried out using a split Hopkinson pressure bar. To reiterate, laser—induced failure by plugging depends on the incident laser indensity and duration ,the spatial profile of the laser beam and their relation to the geometric and material characteristics of the specimen.

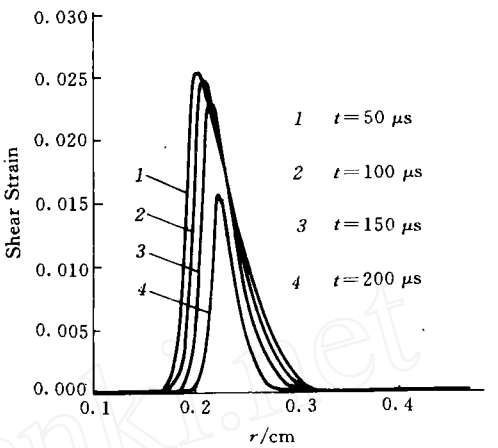

Fig. 15 Transient average shear strain γ vs the radial coordinate for the non—Gaussian type of laser beam with E_J =10J at different time in the case of $D \neq D_0$.

4 Acknowledgements

Authors would like to express their sincere thanks to Prof. Z. M. Chen for his many helpful discussions during the preparation of this paper. Support for this research program was provided partly by NNSF of China and partly by the Field of Laser Technology, 863—NHT Research Development Program. Their support is also gratefully acknowledged.

References

1 Kar A Mazumder J. Two—dimensional model for material damage due to melting and vaporization during laser irradiation. J Appl Phys, 1990,68(8): 1884～3891.

2 Garrison J N. Thermal stresses as laser heating damage mechanism. AD/A 034877. 1976.

3 Chan C L, Mazumder J. One dimensional steady—state model for damage by vaporization and liquid expulsion due to laser—material interaction. J Appl Phys, 1987,62(11):4579～4586.

4 Smurov I, Covelli L, Tagirov K, Aksenov L. Peculiarities of pulse laser alloying: influence of spatial distribution of the beam. J Appl Phys, 1992,71(7):3147～3158.

5 Zweig A D. A thermo—mechanical model for laser ablation. J Appl Phys,1991,70(3):1684～1691.

6 Eliezer S, Gilath I, Bar—Noy T. Laser induced spall in metals:experiment and simulation. J Appl Phys, 1990,67

(2):715～724.

7 Boustie M, Cottet F. Experimental and numerical study of laser induced spallation into aluminum and copper targets. J Appl Phys,1991,69(11):7533～7538.

8 Larson A R. Calculation of laser induced spall in aluminum targets,LA 6189M,1975.

9 Fox J A, Barr D N. Laser－induced shock effects in plexiglass and 6061－T6 aluminum. Appl Phys Lett, 1973,22(11):594～596.

10 Shoukry M, Nair S, Kalpakjian S. Effect of shear deformation on the dynamic plastic bending of metallic plates during normal penetration. Int J Engng Sci, 1991,29(9):1035～1052.

11 Anderson C E, Bodner S R. Ballistic impact:the status of analytical and numerical modeling. Int J Impact Engng, 1988,7(1):9～35.

12 Liss J, Goldsmith W, Kell J M. A phenomenological penetration model of plates. Int J Solids Struct, 1983,1(2):321～341.

13 Jenq S T, Goldsmith W, Kell J M. Effect of target bending in normal impact of a flat－ended cylindrical projectile near the ballistic limit. Int J Solids Struct. 1988,24(2):1243～1266.

14 Duan Z P, Zhou Y C, Xie B M. On laser－induced reverse plugging effect, In: Zheng,Z M. In Proceedings of IUTAM Symp on Impact Dyn. peking:Peking University Press,1994,176～186.

15 Zhou Y C, Duan Z P. Shear deformation analysis of laser－induced reverse plugging effect, Submitted to Int J Non－Linear Mechanics,1996.

16 Berger H M. A new approach to the analysis of large deflections of plates. J Appl Mech, 1965,22:465～742.

17 Ohnable H, Mizuguchi F. Larger deflections of heated nonhomogeneous circular plates with radial varying rigidity. J Non－Linear Mech, 1993,28:365～372.

18 Bhimaraddi A, Chandrashekhara K. Nonlinear vibrations of heated antisymmetric angle－ply laminated plates. Int J Solids Structures, 1993,30:1255～1268.

博士论坛

一种新的破坏模式:反冲塞*

周益春[1,2] 段祝平[2] 杨奇斌[1]

【摘要】 观察到了长脉冲激光束辐照到铜薄片上产生的新的破坏模式.这种破坏可以分为三个阶段:鼓包,剪垣变形局部化及由冲塞所引起的贯穿,这种破坏模式的典型特征是鼓包和冲塞都是沿着入射激光相反的方向进行的,它同人们所塾知的激光引起材料破坏的分裂、烤化和汽化等不同,激发束的特殊的空间分布造成了这种新的破坏模式.

主题词:激光;破坏;反冲塞

分类号:TN249

* 国家 863 计划资助项目

作者单位:1)湘潭大学物理系,湘潭,411105;2)中国科学院力学研究所,材料动力学及激光与物质相互作用实验室

收稿日期:1996－05－06

(第 18 卷完)